Available online at www.sciencedirect.com
SCIENCE DIRECT®
Journal of the European Ceramic Society 25 (2005) 29–36
www.elsevier.com/locate/jeurceramsoc

Bridging stresses in sintered reaction-bonded Si_3N_4 from COD measurements

T. Fett [a], D. Munz [a], A. B. Kounga Njiwa [b], J. Rödel [b,*], G. D. Quinn [c]

[a] *Forschungszentrum Karlsruhe, Institut für Materialforschung II, Postfach 3640, D-76021 Karlsruhe, Germany*
[b] *Darmstadt University of Technology, Institute of Materials Science, Petersenstr. 23, 64287 Darmstadt, Germany*
[c] *Ceramics Division, National Institute for Standards and Technology, Gaithersburg, MD 20899, USA*

Received 24 September 2003; received in revised form 26 February 2004; accepted 6 March 2004
Available online 20 May 2004

Abstract

Crack opening displacement measurements on a sintered reaction-bonded Si_3N_4 ceramic obtained in bending tests with edge-V-notched specimens were evaluated. A procedure is proposed which allows a straight-forward evaluation of the experimental results in order to obtain the bridging stresses as a function of crack opening displacements. Bridging stresses up to 160 MPa were found acting over a distance of about 0.4 μm. In addition crack profile measurements were performed for Vickers indentation cracks which could approximately be described by use of the bridging relation obtained.

Keywords: Si_3N_4; Toughness and toughening; Fracture

1. Introduction

Many ceramics, especially coarse-grained or fibre reinforced materials show an R-curve effect which is caused by crack-face interactions in the wake of an advancing crack. The observed R-curves have often been described by a relation $K_R = f(\Delta a)$. This would be an appropriate description if the R-curve were a pure material property. In the past it has been shown by experimental and theoretical investigations that the R-curve is not a unique material property. The shape of the curve depends on the geometry of the test specimens, the initial crack depth, the type of loading (tension, bending, point forces) and on the special type of crack extension (stable and sub-critical crack propagation).[1]

It is the common opinion that in the special case of R-curves caused by grain bridging effects, the relation between the bridging stresses and crack opening displacement, $\sigma_{br} = f(\delta)$, is the intrinsic material property which is expected to be much less influenced by test conditions.[2,3]

Different methods have been applied to determine the bridging law. Direct measurements of the loads transferred by the bridges were done by Hay and White[4] who developed the post-fracture tensile (PFT) test which gives the crack closure stress versus the crack opening displacement relationship. Pezzotti et al.[5,6] measured the bridging stresses in Si_3N_4 with the use of Raman spectroscopy.

An accurate albeit cumbersome method to determine the bridging stress relation is the evaluation of crack opening displacement (COD) measurements. For coarse-grained alumina often scanning electron microscopes (SEM) were used.[7–9] Measurements with an atomic force microscope (AFM) were presented in Raddatz et al.[10] for $A1_2O_3$/A1 composites and in Meschke et al.[11] and Förderreuther et al.[12] for barium titanate and zirconia.

It is the aim of this paper to evaluate COD measurements for a sintered reaction-bonded Si_3N_4 ceramic. COD data in combination with an elaborate mathematical procedure were used before to compute the starting point of the R-curve, K_{I0}, also called the crack-tip toughness was determined for this material in Kounga Njiwa et al.[13] The K_{I0} value for this material was found to be 1.7 MPa $m^{1/2}$. This value appeared to contradict the fracture toughness found using standardised techniques,[14] which yielded numerical values higher than 5 MPa $m^{1/2}$. The current paper therefore focuses on the determination of the bridging stresses with particular emphasis to short cracks and on the determination of the

* Corresponding author. Tel.: +49-6151-166316; fax: +49-6151-166314.
E-mail address: roedel@ceramics.tu-darmstadt.de (J. Rödel).

0955-2219/$ – see front matter © 2004 Elsevier Ltd. All rights reserved.
doi:10.1016/j.jeurceramsoc.2004.03.005

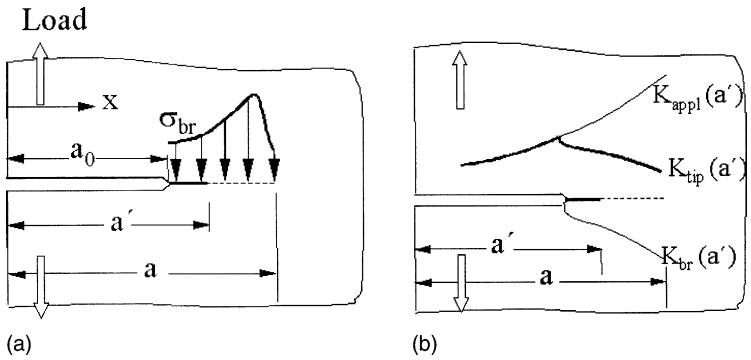

Fig. 1. Crack of length a developed from a notch of length a_0, (a) geometric data and bridging stresses, (b) development of stress intensity factors for a virtual crack of length a.

computation of the resulting R-curve. This work thereby delivers the missing link between crack-tip toughness and standardised fracture toughness evaluations, which are based on instability of finite size cracks (range of about 50–200 μm).

2. Evaluation procedure

An improved evaluation of COD measurements was proposed in Kounga Njiwa et al.[13] and Fett[15] based on the Rice equation,[16] which in integral representation reads

$$\delta_{\text{total}}(x) = \frac{1}{E'}\int_x^a K_{\text{tip}}(a')h(a', x)\,\mathrm{d}a' \tag{1}$$

with coordinate in crack direction x and crack length a both starting from the crack mouth and the weight function $h(a'x)$ that can be found in Kounga Njiwa et al.[13] The integration variable a' varies in the range $a_0 \le a' \le a$ (a_0 = notch depth). An illustration of the geometric data is provided in Fig. 1a. The total stress intensity factor K_{tip}, is the physically effective value at the crack tip and can be obtained by superposition of the (opening) applied stress intensity factor K_{appl} caused by the external load and the (closing) bridging stress intensity factor K_{br} resulting from the so-called bridging stresses σ_{br} (Fig. 1b),

$$K_{\text{tip}} = K_{\text{appl}} + K_{\text{br}}, \quad K_{\text{br}} < 0 \tag{2}$$

with

$$K_{\text{br}}(a') = \int_{a_0}^{a'} \sigma_{\text{br}}(x)h(x, a')\,\mathrm{d}x \tag{3}$$

Fig. 1b illustrates the stress intensity factors $K_{\text{appl}}(a')$, $K_{\text{br}}(a')$, and $K_{\text{tip}}(a')$ for a virtual crack of length a' "growing" into the bridging stress field which is caused by the real crack of length a. A series expansion of the stress intensity factor at the tip of a virtual crack $K_{\text{tip}}(a')$ at $a' = a_0$ yields after truncation at the term with $n = N$.[13]

$$K_{\text{tip}}(a') = K_{\text{appl}}(a') + \sum_{n=1}^{N} B_n(a' - a_0)^{n/2} \tag{4}$$

where the applied stress intensity factor for the virtual crack length a' is given by

$$K_{\text{appl}}(a') = K_{\text{appl}}(a)\frac{Y(a')}{Y(a)}\sqrt{\frac{a'}{a}} \tag{5}$$

with $K_{\text{appl}}(a)$ externally applied during the COD measurements. $Y(a)$ denotes the fracture mechanics geometry function defined as

$$K_{\text{appl}}(a) = \sigma Y(a)\sqrt{a} \tag{6}$$

where σ is a characteristic stress, e.g. the outer fibre bending stress. The crack-tip toughness K_{I0} is identical with the total stress intensity factor at $a' = a$.

Consequently, Eq. (4) results in

$$\delta_{\text{total}}(x) = \frac{K_{\text{I0}}}{E'}\int_x^a h(a', x)\,\mathrm{d}a' + \frac{1}{E'}\sum_{n=1}^{N} B_n J_n(a, x) \tag{7}$$

The integrals J_n read

$$J_n(a, x) = \int_x^a (a' - a_0)^{n/2}h(a', x)\,\mathrm{d}a' \tag{8}$$

with the weight function h. A least-squares routine applied to measured crack opening displacements yields a sufficient number of coefficients B_n from Eqs. (4) and (7).

3. Material and measurements

The sintered reaction-bonded silicon nitride (SRBSN)[1,2] used for this study was a commercial material containing yttria and alumina. The material is in full-scale production for several applications including cam roller followers in a

[1] Ceralloy 147-31N, Ceradyne, Cosa Mesa, CA.

[2] Certain commercial materials or equipment are identified in this paper to specify adequately the experimental procedure. Such identification does not imply endorsement by the Forschungszentrum Karlsruhe, Darmstadt Technical University, nor the National Institute of Standard and Technology nor does it imply that these materials or equipment are necessarily the best for the purpose.

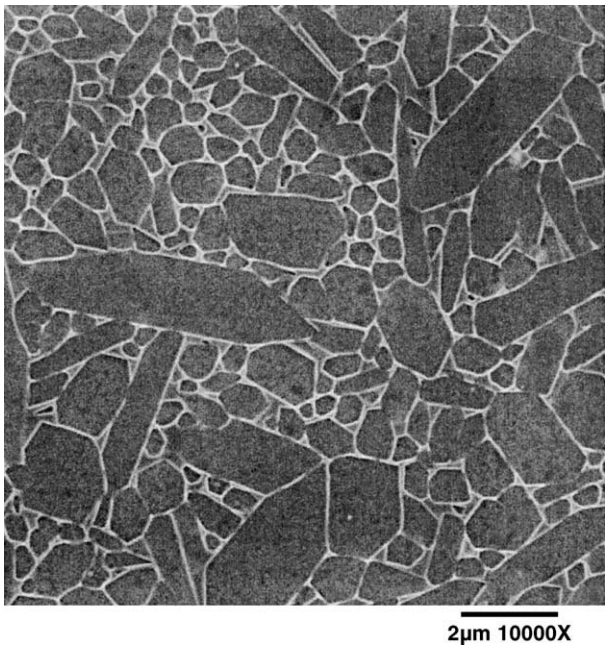

Fig. 2. Microstructure of the SRBSN as revealed on polished and etched surface.

diesel engine and pump valve components for the oil extraction industry. This SRBSN has needle-like beta silicon nitride grains, 0.5–3 μm wide by up to 10 μm long, bonded by a second phase as illustrated in Fig. 2. The material was designed to have enhanced fracture toughness. The manufacturer lists the elastic modulus as 310 GPa, the strength as >700 MPa, density as 3.21 g/cm^3, and the Vickers hardness as 17.6 and 15.4 GPa at 49 and 2.9 N indentation loads, respectively. With a Poisson's ratio of $v = 0.28$ the plane strain Young's modulus necessary for the displacement computations results as $E' = 310/(1 - 0.28^2)$ GPa.

Silicon starting powders were isopressed into oversized green-body rods that were nitrided and then gas pressure sintered to a final size of 7.5 mm in diameter by 111 mm long after sintering. The manufacturer reported the fracture toughness as between 5.5 and 6.5 MPa m$^{1/2}$.[17] New results using the three methods in ASTM standard C 1421-99[18] (single-edge pre-cracked beam, chevron-notched beam, and surface crack in flexure) produced very consistent results from 5.3 to 5.6 MPa m$^{1/2}$ on average.[14] Standard rectangular bend specimens of size 3 mm × 4 mm × 45 mm were sliced and ground from these blanks.

A V-notch of approximately 1 mm length and notch root radius of about 10 μm was cut on the edge of a specimen (Fig. 3b) using the razor blade method.[19,20] The sample was mounted into a self-designed SEVNB-testing apparatus (Fig. 3a) and placed under an optical microscope.[21] The externally applied load was gradually increased until a sharp through-thickness crack arose. After a stable crack extension of 0.52 mm the applied $K = 5.9$ MPa m$^{1/2}$ was evaluated using the maximum load, the specimen dimensions, and the crack size according to the relationship in the German Draft Standard DIN 51′109.[22] The specimen was subsequently unloaded and removed from the testing device. A thin Au/Pd film was sputtered onto the polished insulating surface of the ceramic material to allow further measurements in an SEM. The SEM was modified such that in situ COD measurements could be run at controlled externally applied loads. The sputtered edge-cracked specimen was then mounted again in the SEVNB-loading device, partially loaded, and placed into the SEM, thus enabling the crack to be opened up during measurement of the crack profile. In order to avoid significant sub-critical crack growth, profiles were measured at applied loads, that represented 97, 90 and 80%, respectively, of the load required for the very last crack extension in the optical microscope. An appropriate software was used for the evaluation of the CODs. The resulting data were then extrapolated into crack opening displacements related to the full load as applied during the prior stable crack extension phase.[13]

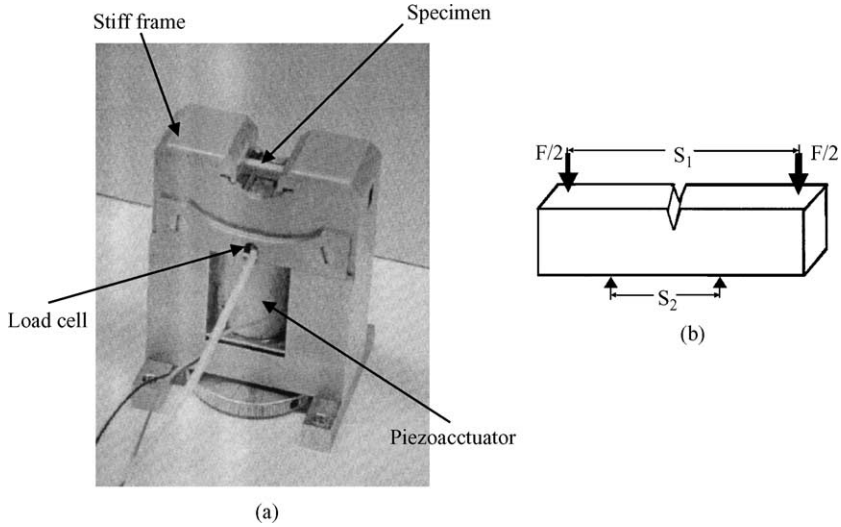

Fig. 3. (a) SEVNB-testing apparatus and (b) bend bar geometry with V-notch cut on the edge.

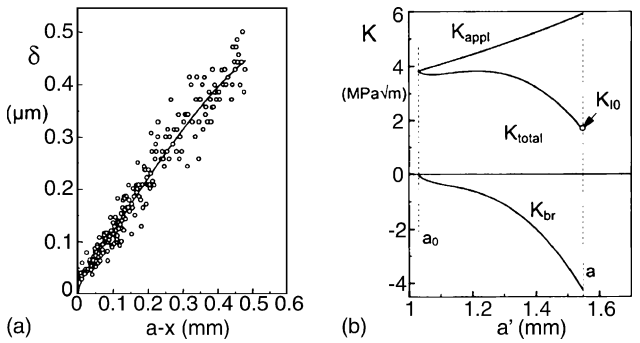

Fig. 4. (a) Total crack opening displacements for a crack with crack extension $\Delta a = 0.52\,\text{mm}$ and $K_{\text{appl}} = 5.9\,\text{MPa}\,\text{m}^{1/2}$, (b) representation of the three stress intensity factors K_{appl}, $K_{\text{tip}}(a')$, and K_{br}.

Fig. 4a shows COD measurements evaluated in Kounga Njiwa et al.[13] which provide the coefficients compiled in Table 1 using Eqs. (4)–(8). Within the scatter of measurement, the results can be represented by

$$\delta = \sqrt{\frac{8}{\pi}}\frac{K_{\text{I0}}}{E'}\sqrt{a-x} + 0.048(a-x)^{3/2} - 43.23(a-x)^{5/2} \tag{9}$$

with $K_{\text{I0}} = 1.7\,\text{MPa}\,\text{m}^{1/2}$ and δ and $a - x$ in meters.

4. Bridging stresses

4.1. Determination of the bridging relation

The parameters in Table 1 may be used to estimate the bridging stress relation $\sigma_{\text{br}} = f(\delta_{\text{total}})$. From the preceding considerations we know the total stress intensity factor K_{tip} as a function of an arbitrary virtual crack length $a_0 \le a' \le a$. Also the applied stress intensity factor K_{appl} is known, $K_{\text{appl}} = 5.9\,\text{MPa}\,\text{m}^{1/2}$.

The bridging stress intensity factor $K_{\text{br}}(a')$ is obtained from the total and the applied ones by superposition as

$$K_{\text{br}}(a') = K_{\text{tip}}(a') - K_{\text{appl}}(a'), \quad K_{\text{br}} < 0 \tag{10}$$

Fig. 4b gives the total stress intensity factor computed by Eq. (4), the applied stress intensity factor according to Eq. (5), and the bridging stress intensity factor derived from Eq. (10). Replacing the bridging stress intensity factor by its integral representation

$$\int_{a_0}^{a'} \sigma_{\text{br}}(x)h(a',x)\,\mathrm{d}x = K_{\text{tip}}(a') - K_{\text{appl}}(a') \tag{11}$$

yields a Volterra integral equation of first kind with kernel $h(a'x)$, which can be solved with the usual methods providing $\sigma_{\text{br}}(x)$. Two methods were applied to solve Eq. (11).

In the first approach to solve Eq. (11), the stress distribution $\sigma_{\text{br}}(x)$ was represented by a number of $M = 100$ stress values at equidistant locations $a_0 < a < a$. The stress values $\sigma_{\text{br}}(x_1)$, $\sigma_{\text{br}}(x_2)$, …, $\sigma_{\text{br}}(x_M)$ were interpolated by cubic splines to get a continuous distribution. In a subroutine the integrals were evaluated by application of Simpson's rule. In a least-squares routine the M stress values were systematically changed until the sum of squares evaluated for a number of m values a' became minimum, i.e. until

$$\sum_{(m)}\left(\int_{a_0}^{a'}\sigma_{\text{br}}(x)h(a',x)\,\mathrm{d}x - K_{\text{total}}(a') - K_{\text{appl}}(a')\right)^2 = \text{min} \tag{12}$$

was fulfilled in $a_0 < a' < a$ within a prescribed error margin. For the solution of Eq. (12), the authors used the least-squares subroutine VA02AD of the Harwell Subroutine Library.[23] In a second attempt, here outlined in more detail, the unknown bridging stresses were expressed by polynomials

$$\sigma_{\text{br}}(x) = \sum_{m=0}^{M} C_m x^m \tag{13}$$

with unknown coefficients C_m. Finally, the least-squares sum

$$\left(\sum_{n=0}^{N}\int_{a_0}^{a'} x^m h(a',x)\,\mathrm{d}x - K_{\text{br}}(a')\right)^2 = \text{min} \tag{14}$$

has to be minimised. The result is shown in Fig. 5a. Plotting $\sigma_{\text{br}}(x)$ versus $\delta_{\text{total}}(x)$ yields the bridging relation $a_{\text{br}} = f(\delta_{\text{total}})$ as given in Fig. 5b.

These bridging stresses may be represented by the average relations

$$\sigma_{\text{br}} = \sigma_0 \exp\left(\frac{\delta}{\delta_0}\right), \quad \sigma_0 = -177\,\text{MPa}, \quad \delta_0 = 0.22\,\text{m} \tag{15a}$$

$$\sigma_{\text{br}} = \sigma_0\left(\frac{1-\delta}{\delta_0}\right), \quad \sigma_0 = -165\,\text{MPa}, \quad \delta_0 = 0.35\,\text{m} \tag{15b}$$

which are plotted in Fig. 5b as the dashed and dash-dotted line, respectively.

Table 1
Coefficients for Eq. (4) describing the data in Fig. 4

K_{I0} (MPa m$^{1/2}$)	B_1 (MPa)	B_2 (MPa m$^{-1/2}$)	B_3 (MPa^{-1})	B_4 (MPa m$^{-3/2}$)
1.65	−16.9	−9599	1.194×10^6	-4.793×10^7

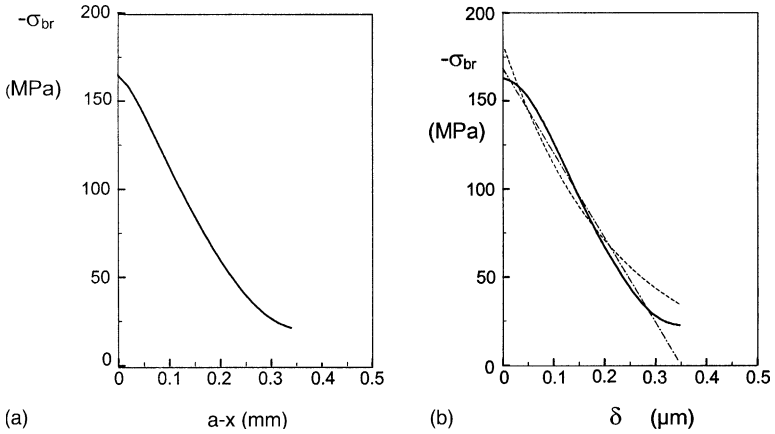

Fig. 5. Bridging stresses (a) as a function of the location, (b) as a function of crack opening, dashed curve: rough approximation of bridging stresses by Eq. (15a), dash-dotted line: Eq. (15b).

There are no other data on effective crack closure stresses available for silicon nitride. This work, however, can be compared with results obtained by Pezzotti et al.[5,6] who determined grain-localised bridging stresses in two highly toughened silicon nitride materials. These materials had plateau toughness values of 11 MPa $m^{1/2}$ [5] and 15 MPa $m^{1/2}$,[6] respectively. Localised bridging stresses of 500–1000 MPa were observed at a distance less than 80 μm from the crack tip with localised closure stresses of 100–500 MPa at a distance to the crack tip between 80 and 800 μm. The area fraction of bridging grains multiplied with the localised bridging stresses will yield the average closure stress for a given crack opening displacement. Therefore, considering that the materials in[5,6] have different plateau toughness, the averaged closure stresses and the localised closure stresses appear to be quite consistent.

4.2. Computation of the R-curve

Knowledge of the bridging stress relation allows determination of the R-curve. The bridging contribution to the R-curve value K_R represented by the applied stress intensity factor

$$K_R = K_0 - K_{br} \tag{16}$$

results in

$$K_{br} = \int_{a_0}^{a} \sigma_{br}(x) h(a, x)\, dx \tag{17}$$

The bridging stresses as a function of total crack opening displacement are available from the solid curve in Fig. 5b. Due to Eq. (7) we can transform the displacement dependency $\sigma_{br}(x)$ into a location dependency $\sigma_{br}(x)$. Introducing these stresses into Eq. (15) and performing the integration yields the bridging stress intensity factor as plotted in Fig. 6a by the solid curve. Fig. 6b shows the total R-curve obtained by adding the K_{I0} value of 1.7 MPa $m^{1/2}$. Two crack extensions of $\Delta a = 0.23$ and 0.52 mm were evaluated for the identical material.[13] The related applied stress intensity factors were introduced in Fig. 6 as the squares, where a good agreement between the calculated K_r and the measured K_{appl} can be obtained. In order to reduce the numerical effort it is recommended to use an approximate solution as proposed in Fett et al.[24,25] For small crack extensions and an exponentially decreasing bridging stress relation as given by Eq. (15a),

$$k_{br} = K_{br,max}[1 - \exp(-D\sqrt{\Delta a})] \tag{18}$$

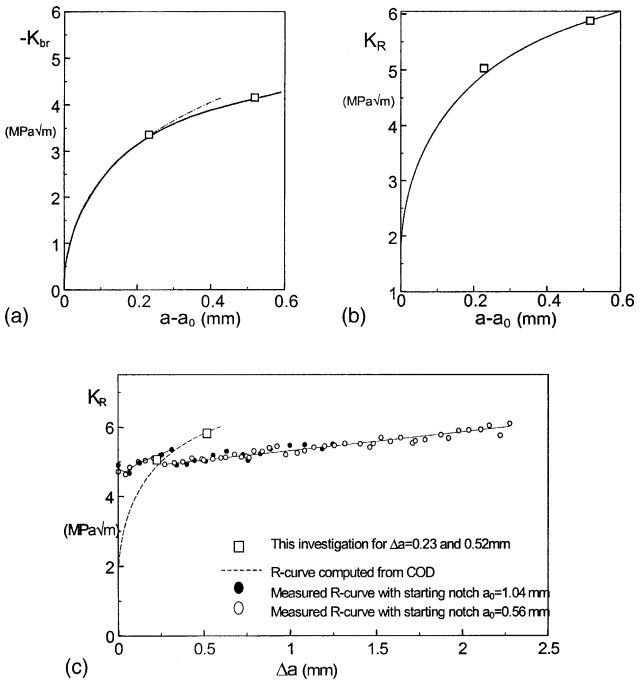

Fig. 6. (a) Bridging stress intensity factor computed with the bridging relation, Fig. 5b (solid curve), near-tip approximation Eq. (18) (dash-dotted curve), (b) total R-curve (measured values from Kounga Njiwa et al.[13] as squares), (c) results of Fig. 4b compared with two further R-curve results obtained for the same material.

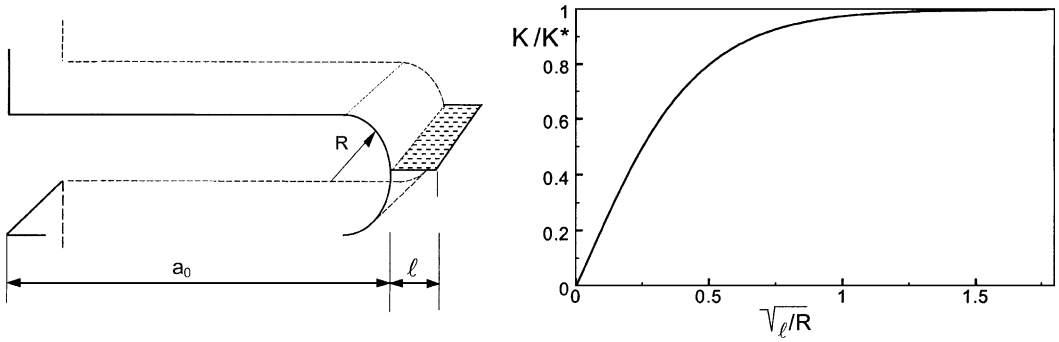

Fig. 7. Crack ahead of a slender notch (a) geometric data, (b) true stress intensity factor K and formally computed "apparent" stress intensity factor K^* according to Eq. (20).

with

$$K_{\mathrm{br,max}} = \sigma_0 \frac{E'\delta_0}{K_{\mathrm{I0}}} \cong -8\,\mathrm{MPa\,m^{1/2}},$$

$$D = \sqrt{\frac{8}{\pi}}\frac{K_{\mathrm{I0}}}{E'\delta_0} \cong 35\,\mathrm{m^{1/2}} \tag{19}$$

The result given by (18) is plotted in Fig. 6a by the dashed curve. The agreement with the full solution is good up to $a - a_0 \approx 0.3$ mm.

In Fig. 6c two additional R-curves obtained on V-notched bending specimens are plotted as the circles. K_{R} values of 5–6 MPa m$^{1/2}$ were found as reported earlier from the conventional chevron-notched beam, single-edged precracked beam and surface crack in flexure methods.[14,17,18] In these measurements the steep increase of the R-curve is not visible. A starting point of the R-curve at $K_{\mathrm{R}} \approx 4.7$ MPa m$^{1/2}$ is visible which is in clear contrast to the $K_{I0} \approx 1.7$ MPa m$^{1/2}$ found from COD evaluation. This may be a consequence of the fact that in conventional crack growth tests the first crack extension is the propagation of a small crack with length ℓ from a notch of length a_0.

In the evaluation of the R-curve experiments an edge-crack of length $a = a_0 + \ell$ is assumed to exist (for the geometric data see Fig. 7a), and the formally computed "apparent stress intensity factor" is commonly computed as

$$K^* = \left(\sigma_{\mathrm{bend}}\sqrt{\pi(a_0+1)}\right) F_{\mathrm{band}}\left(\frac{a}{W}\right) \tag{20}$$

where F_{bend} is the geometric function for a specimen of width W under the applied load, here for instance under bending load.The stress intensity factor given by Eq. (20) is of course a correct value in cases where the crack length ℓ is clearly larger than the radius R of the notch. But in the first crack extension phase where the crack length ℓ is comparable to R, Eq. (20) does not represent the correct stress intensity factor value. In this case the fracture mechanics problem of a small crack in front of a finite notch has to be considered. In the special case of an edge crack ahead of a slender notch with R small compared to the crack length and the other specimen dimensions, the true stress intensity factor K is given by[26]

$$K \cong K^* \tanh[2.243\sqrt{\ell/R}] \tag{21}$$

This relation is shown in Fig. 7b. From this plot it is clearly visible that the true stress intensity factor is significantly lower than the formally computed values K^*. Eq. (19) makes clear, why the starting point of the apparent R-curve, K^*_{I0}, must be larger than the true K_{I0}, namely

$$K^*_{\mathrm{I0}} \cong \frac{K^*}{\tanh[2.243\sqrt{\ell/R}]} > K^* \tag{22}$$

For the differences in K_{I0} and K^*_{I0} obtained for coarse-grained alumina see also Kounga Njiwa et al.[26] A more detailed analysis of the notch effect on the R-curve is given in Fett.[27]

The R-curve in silicon nitride has often been reported as very steep in the first 100 μm, providing a toughness increment of 4–9 MPa m$^{1/2}$,[5,6,28] depending on material and final plateau toughness. The high toughness increment in the first crack extension was also classified as a "pop-in" crack extension due to elastic bridging, which is so close to the crack tip, that it can be considered an intrinsic property itself.[5] It is therefore not surprising that this toughening contribution can be measured with the technique of evaluating the crack opening displacement, but cannot be resolved with crack propagation studies from a sharp notch as found in our study.

The problem of requiring very sharp notches to avoid an influence of notch root radius on apparent fracture toughness is well-known.[29] However, even notch radii of less than 5 μm[30] yielded fracture toughness values for a particular silicon nitride of 4.7 MPa m$^{1/2}$ and thereby a much higher value than all measurements for crack-tip toughness in silicon nitride performed before.[5,13] These obtained fracture toughness values then signify only the instability point of the R-curve in the configuration of bend bar with through-thickness crack. Furthermore, even, if the first crack extension from an SEVNB notch can be captured, the first toughness values are high.[21] This has been demonstrated in a comparison of SCF curves and SEVNB R-curves in alumina–zirconia laminates,[21] where the starting point of an R-curve starting from a very sharp notch lies higher than the

values for short SCF R-curves. The notch tip effect modelled above, therefore, has received considerable experimental justification.

4.3. Vickers indentation cracks

Since the bridging stresses are available from the edge crack measurements, let us now compute the bridging displacements and total displacements for the Vickers indentation crack. For a half-penny-shaped surface crack of depth a, loaded by the bridging stress field $\sigma_{\mathrm{br}}(r)$, the bridging crack opening displacements δ_{br} are given as

$$\delta_{\mathrm{br}}(r) = \frac{4}{\pi E'} \int_r^a \left(\int_0^{a'} \frac{r' \sigma_{\mathrm{br}}(r')}{\sqrt{a'^2 - r'^2}} \mathrm{d}r' \right) \frac{\mathrm{d}a'}{\sqrt{a'^2 - r^2}} \tag{23}$$

with the radial coordinate r and the Young's modulus for plane strain E'. The "applied displacements" δ_{appl} are then given by superposition of the measured total displacements and the bridging displacements as

$$\delta_{\mathrm{appl}} = \delta_{\mathrm{total}} - \delta_{\mathrm{br}} \tag{24}$$

Measured total displacements for a Vickers indentation crack are shown in Fig. 8b as the open circles. From these data and the bridging stress relation, Fig. 5b, the bridging stresses as a function of the radial coordinate, $\sigma_{\mathrm{br}}(r)$, are known. Integration according to Eq. (23) results in the bridging displacements plotted in Fig. 8a. The applied displacements computed by Eq. (24) are shown in Fig. 8b as the full circles.

The displacements caused by the residual stresses in the vicinity of the Vickers indentation were computed.[31] The displacements (interpreted here as the applied ones) can be approximated for $r > b$ (where b is the radius of the inner semi-circle where the two crack surfaces are in contact) by

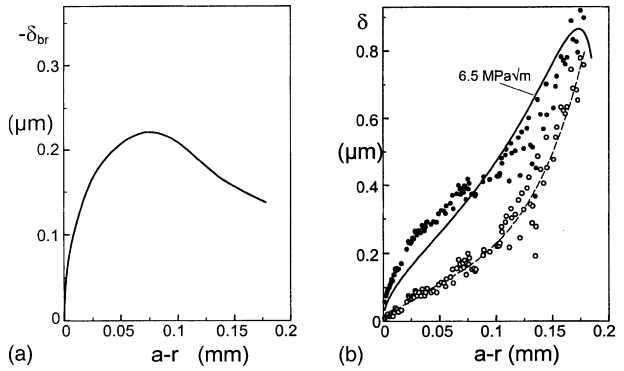

Fig. 8. (a) Bridging displacement distribution, (b) applied displacements (solid circles) computed by superposition of total and bridging displacements compared with applied COD computed from Eq. (18) for $K_{\mathrm{appl}} = 6.5\,\mathrm{MPa\,m^{1/2}}$ (full line). Open circles represent the measured total displacements of a Vickers radial crack in the investigated material.

$$\delta_{\mathrm{appl}} = \frac{4K_{\mathrm{appl}}\sqrt{a}}{0.382\pi E'} \left(\frac{a}{b}\right)^2 \left[\frac{b}{2a} g_2(a,b,r) + \left(\frac{0.635 + 0.319b}{a} \right) g_1(a,b,r) - g_1(a,\lambda b,r) \right] \tag{25}$$

with

$$g_1(a,b,r) = \sqrt{1 - \left(\frac{r}{a}\right)^2} \left(1 - \sqrt{1 - \left(\frac{b}{a}\right)^2} \right) + \frac{r}{a} \left[\boldsymbol{E}\left(\left(\frac{b}{r}\right)^2 \right) - E\left(\arcsin\frac{r}{a}, \left(\frac{b}{r}\right)^2 \right) - \left(1 - \left(\frac{b}{r}\right)^2\right) \left(\boldsymbol{K}\left(\left(\frac{b}{r}\right)^2 \right) - F\left(\arcsin\frac{r}{a}, \left(\frac{b}{r}\right)^2 \right) \right) \right] \tag{26a}$$

$$g_2(a,b,r) = \frac{b}{r} \left[\boldsymbol{E}\left(\left(\frac{b}{r}\right)^2 \right) - E\left(\arcsin\left(\frac{r}{a}, \left(\frac{b}{r}\right)^2\right) \right) \right] \tag{26b}$$

where $\boldsymbol{E}$ and $\boldsymbol{K}$ are the complete and E and F the incomplete elliptical integrals. The parameter λ can be expressed by

$$\lambda \cong 0.9828 \left(\frac{a}{b}\right)^{0.00565} \tag{27}$$

This solution is additionally introduced in Fig. 8b for $K_{\mathrm{appl}} = 6.5\,\mathrm{MPa\,m^{1/2}}$ as the solid curve which roughly agrees with the solid circles. Whereas for the near-tip region the data points are underestimated, the data in larger distance from the crack tip are slightly overestimated. From this result we can estimate the R-curve value corresponding to a Vickers indentation crack as $K_R \approx 6.5\,\mathrm{MPa\,m^{1/2}}$.

5. Conclusions

COD measurements on an edge-notched bending bar were carried out after a stable crack extension of about 0.5 mm. From these results bridging stresses as a function of crack opening displacements could be determined by a straightforward procedure. It was found that

- maximum bridging stresses σ_{br} of about 160 MPa were obtained at small COD,
- bridging interactions become negligible for displacements $\delta > 0.4\,\mu\mathrm{m}$,
- measured R-curves in the first 200 μm of crack extension lie higher than R-curves predicted from the bridging law. This is attributed to finite-width notch effects,
- the crack profile for a Vickers indentation test can roughly be interpreted with this bridging behaviour.

Acknowledgements

This study was supported by the Deutsche Forschungsgemeinschaft under Rö 954/15 and Fe 509/15. W. Luecke of NIST is thanked for the microstructure image.

References

1. Steinbrech, R., Knehans, R. and Schaarwächter, W., Increase of crack resistance during slow crack growth in $A1_2O_3$ bend specimens. *J. Mater. Sci.* 1983, **18**, 265–270.
2. Fett, T. and Munz, D., Influence of crack-surface interactions on stress intensity factor in ceramics. *J. Mater. Sci. Lett.* 1990, **9**, 1403–1406.
3. Cox, B. N. and Marshall, D. B., Stable and unstable solutions for bridged cracks in various specimens. *Acta Metall.* 1991, **39**, 579.
4. Hay, J. C. and White, K. W., Grain-bridging mechanisms in monolithic alumina and spinel. *J. Am. Ceram. Soc.* 1993, **76**, 1849–1854.
5. Pezzotti, G., Muraki, N., Maeda, N., Satou, K. and Nishida, T., In situ measurement of bridging stresses in toughened silicon nitride using Raman microprobe spectroscopy. *J. Am. Ceram. Soc* 1999, **82**, 1249–1256.
6. Pezzotti, G., Ichimaru, H. and Ferroni, L., Raman microprobe evaluation of bridging stresses in highly anisotropic silicon nitride. *J. Am. Ceram. Soc.* 2001, **84**, 1785–1790.
7. Rödel, J., Kelly, J. F. and Lawn, B. R., In situ measurements of bridged crack interfaces in the scanning electron microscope. *J. Am. Ceram. Soc.* 1990, **73**, 3313–3318.
8. Fett, T., Munz, D., Seidel, J., Stech, M. and Rödel, J., Correlation between long and short crack R-curves in alumina using the crack opening displacement and fracture mechanical weight function approach. *J. Am. Ceram. Soc.* 1996, **79**, 1189–1196.
9. Seidel, J. and Rödel, J., Measurement of crack-tip toughness in alumina as a function of grain size. *J. Am. Ceram. Soc.* 1997, **80**, 433–438.
10. Raddatz, O., Schneider, G. A., Mackens, W., Voß, H. and Claussen, N., Bridging stresses and R-curves in ceramic/metal composites. *J. Eur. Ceram. Soc.* 2000, **20**, 2261–2273.
11. Meschke, F., Raddatz, O., Kolleck, A. and Schneider, G. A., R-curve behaviour and crack-closure stresses in barium titanate and (Mg, Y)-PSZ ceramics. *J. Am. Ceram. Soc*. 2000, **83**, 353–361.
12. Förderreuther, A., Thurn, G., Zimmermann, A. and Aldinger, F., R-curve effect influence of electric field and process zone in $BaTiO_3$ ceramics. *J. Eur. Ceram. Soc.* 2002, **22**, 2023–2031.
13. Kounga Njiwa, A. B., Fett, T., Rödel, J. and Quinn G., Crack-tip toughness measurements on sintered reaction-bonded Si_3N_4. *J. Am. Ceram. Soc.*, in print.
14. Quinn, G. D., Swab, J. J. and Motyka, M. J., Fracture toughness of a toughened silicon nitride by ASTM C. *J. Am. Ceram. Soc.* 2003, **86**, 1043–1045.
15. Fett, T., Crack-tip toughness from wide-range COD measurements. *Int. J. Fract.* 2002, **114**, L29–L32.
16. Rice, J. R., Some remarks on elastic crack-tip stress fields. *Int. J. Solids Struct.* 1972, **8**, 751–758.
17. Mikijelj, B. and Mangels, J., SRBSN material development for automotive applications. In *Ceramic Materials and Components for Automotive Applications*, ed. J. G. Heinrich and F. Aldinger. Wiley-VCH, 2001, pp. 393–398.
18. ASTMC 1421-99, Standard test method for the determination of fracture toughness of advanced ceramics. *Annual Book of Standards, Vol 15.01*. American Society for Testing and Materials, West Consho-hocken, PA, USA, 2001.
19. Nishida, T., Pezzotti, G., Mangialardi, T. and Paolini, A. E., In *Fracture Mechanics Evaluation of Ceramics by Stable Crack Propagation in Bend Bar Specimens*, ed. R. C. Bradt, D. P. H. Hasselman, D. Munz, M. Sakai and V. Y. Shevchenko. *Fract. Mech. Ceram.* 1996, **11**, 107–114.
20. Kübler, J., Fracture toughness using the SEVNB method: preliminary results. *Ceram. Eng. Sci. Proc.* 1997, **18**, 155–162.
21. Moon, R., Bowman, K., Trumble, K. and Rödel, J., Comparison of R-curves from single-edge V-notched beam (SEVNB) and surface-crack-in-flexure (SCF) fracture-toughness test methods on multilayered alumina–zirconia composites. *J. Am. Ceram. Soc.* 2000, **83**, 445–447.
22. German Draft Standard DIN 51' 109, *Prüfning Von Keramischen Hochleistungswerkstoffen, Ermittlung der Risszähigkeit* K_{Ic}. German Institute of Standards, Berlin, September 1991.
23. Harwell Subroutine Library, *A Catalogue of Subroutines*. Computer Science and Systems Division, AERA, Harwell, 1981.
24. Fett, T., Munz, D., Geraghty, R. D. and White, K. W., Influence of specimen geometry and relative crack size on the R-curve. *Eng. Fract. Mech.* 2000, **66**, 375–386.
25. Fett, T. and Munz, D., *Stress Intensity Factors and Weight Functions*. Computational Mechanics Publications, Southampton, 1997.
26. Kounga Njiwa, A. B., Yousef, S. G., Fett, T. and Rödel, J., Crack-tip toughness of coarse-grained alumina. *Eng. Fract. Mech.*, submitted.
27. Fett, T., Influence of a finite notch root radius on the measured R-curves. *J. Mater. Sci. Lett.*, to appear.
28. Ramachandran, N. and Shetty, D. K., Rising crack growth resistance (R-curve) behavior of toughened alumina and silicon nitride. *J. Am. Ceram. Soc.* 1991, **74**, 2634–2641.
29. Damani, R., Gstrein, R. and Danzer, R., Critical notch root radius effect in SENB-S fracture toughness testing. *J. Eur. Ceram. Soc*. 1996, **16**, 695–702.
30. Damani, R., Schuster, C. and Danzer, R., Polished notch modification of SENB-S fracture toughness testing. *J. Eur. Ceram. Soc.* 1997, **17**, 1685–1689.
31. Fett, T., Kounga Njiwa, A. B. and Rödel, J., Stresses and stress intensity factor from COD of Vickers indentation cracks. *J. Mater. Sci.* 2004, **39**, 2219–2221.